Optimize Kalman Filter For Smart Phone Location Tracking Using GNSS Measurements

Rishoban Yokanathan

***Abstract*— Point precise positioning (PPP) method allows to locate user with Global Navigation Satellite System under good condition. But this method is quite challenging to locate user when user is in urban areas with obstacles. Another alternative solutions such as Real Time Kinematic solve these problems with differential measurements. In real world scenario, raw GNSS measurements have usually noisy and uncertain data. Kalman filter is successful method to optimally update variables with indirect measurements. This research proposes the method to optimize Kalman filter based PPP to improve smart phone location tracking. Evaluation method showed that proposed method worked well with approximately 3.0 meter accuracy and outperformed base line model which is calculated using Weighted-Least-Square (WLS) solver.**

***Keywords*— GNSS, Kalman Filter, Weighted Least Square, Android, Point Precise Positioning**

I. Introduction

Point Precise Point Precise Positioning(PPP) produces the geodetic positions using Global navigation satellite system(GNSS) constellations. Not like Differential GNSS method, without referential base station PPP locate user positions. Global Navigation Satellite System is a collective term that used to provide 3-D user location, navigation and time services. Based on GNSS signal transmission data, user can calculate the position without transmits any signals. To cover the earth which means a person who is from anywhere in the earth can see at least one satellite, satellites work as group which is called as satellite constellation. There are many satellites constellation is available such as Global Positioning System (GPS), GLONASS, Galileo, BeiDou and QZSS. They may differ from number of satellites orbiting, frequency of transmitting data etc. Every satellite transmits information about the location other relevant data to the receiver. Satellite data always doesn't have higher accuracy. But the use of smartphones with multiple GNSS constellations helps to improve accuracy and solution availability by utilizing signals from multiple satellite systems. For high-accuracy positioning, a stable antenna position is crucial. However, smartphones are in constant motion, leading to changes in attitude (which affects antenna gain), altitude (such as when holding the smartphone close to the body or in front of the face for reading), and obstruction conditions.

Correspondence: Rishoban Yokanathan (E-mail: rishoban27@gmail.com)
Received:08.03.2023 Revised:17.04.2023 Accepted: 19.06.2023

Rishoban Yokanathan is from University of Colombo School of Computing, Sri Lanka. (rishoban27@gmail.com)

DOI: https://doi.org/10.4038/icter.v16i2.7263

However, the antenna's main weakness is its poor ability to suppress multipath interference [17]. Errors happen because of faults in the hardware measurement, environmental factors and earth rotation causing measurement noise and uncertainty. Measurement noise, uncertain data and transmitting error play major role in finding user's location. The expected robust model has to produce accurate location with noisy data.

II. Background

The errors originate from factors such as the quality of satellite orbits and clocks, atmospheric effects, multipath interference, and signal blockages. While code measurements are insufficient for high accuracy, phase measurements are necessary despite their ambiguity.

Traditionally, high-precision GNSS techniques like carrier phase differential and Precise Point Positioning (PPP) have been limited to expensive geodetic dual frequency receivers used in specialized fields. These techniques are commonly employed in geodesy, surveying, engineering, navigation, and geophysics. To enable high-accuracy positioning using single-frequency mass-market chipsets in smartphones, GNSS algorithms optimized for real-time processing are required to address and resolve the error sources.

The differential Static or Kinematic approach utilizes multiple receivers, typically a rover and a reference station or network, to eliminate common GNSS errors. PPP, on the other hand, performs precise positioning with a single receiver by leveraging additional information to mitigate errors. Dual frequency observations greatly benefit both methods. The differential approach relies on nearby reference stations, which are already established in many developed countries. PPP, while not requiring differencing techniques, relies on precise GNSS orbit and clock data products, which are currently limited for single frequency observations.

Navigation errors start from transmission of data and clock errors [10]. Even though, GNSS use high accurate atomic clocks, there are some possibilities to clock error. For example, clock drift. The main reason for the drift is Control Segment doesn't want to constantly tweak the clocks. If there is a 10 nanoseconds of clock error, then results may have 3 metres of position error [5].

But satellites transmit clock related errors such as bias, drift, offset and uncertainty which are monitored by GNSS ground control system.

Ionosphere, troposphere is layer atmosphere on the earth surface. Electrically charged particles such as ions which is in ionosphere caused satellite signal delay and environmental factors such as humidity, temperature which is in troposphere create delay in signal. Environment of the receiver also contribute the accuracy of the position estimation.

For example, environment which has tall buildings or mountains interrupt the signals or reflecting signals and cause multi path interference.

Zenith Total Delay (ZTD), also referred to as Zenith Wet Delay or Zenith Hydrostatic Delay, is a parameter used in meteorology and Global Navigation Satellite System (GNSS) applications. It represents the total delay experienced by a signal traveling from a GNSS satellite through the Earth's atmosphere to a receiver located at the zenith (directly overhead). ZTD consists of two main components: the hydrostatic delay and the wet delay. The hydrostatic delay accounts for the delay caused by the Earth's atmosphere's density and pressure, while the wet delay represents the delay caused by water vapor in the atmosphere. These delays introduce errors in the GNSS measurements and need to be corrected to improve positioning accuracy. By estimating the ZTD, atmospheric corrections can be applied to GNSS signals to mitigate the influence of the atmosphere and improve the accuracy of positioning and weather forecasting. ZTD is typically expressed in units of millimeters or centimeters and is an important parameter in meteorological models and GNSS data processing algorithms.

Benvenuto et al try to assess the feasibility of estimating Zenith Total Delay (ZTD) using GNSS measurements from smartphones [20]. The goal was to explore the potential for local troposphere monitoring. The researchers conducted tests at two different sites using different software for data processing. They compared ZTD estimates obtained from a dual-frequency and multi-constellation receiver embedded in the smartphones with those obtained from a GNSS Continuously Operating Reference Station (CORS). The results demonstrated promising performance in estimating ZTD from smartphones, showing comparable accuracy to estimations obtained with a geodetic receiver. This highlights the potential for using smartphones as a cost-effective tool for ZTD estimation and local troposphere monitoring.

In the Point Precise Positioning, multi path effect is serious problem and it affects quality of the signal then slow down the convergence of PPP. This problem can't be eliminated by establishing mathematical model or differential technology. There are several authors proposed solutions based on hardware design and post-processing methods [11]. Solutions to mitigate multi path effects are classified as antenna, measurement processing, signal decomposition. Antenna design improvements primarily target the lower gain experienced at low satellite elevations. This includes the use of choke-ring antennas and ground planes to enhance the reception quality in challenging environments [11]. To effectively model multipath variation, the measurement processing techniques employed in the aforementioned studies utilize the correlation between multipath and both satellite elevation and signal-to-noise ratio (SNR) measurements. By analyzing these relationships, researchers can better understand and mitigate the effects of multipath interference [12, 13, 14]. Additionally, alternative methods like wavelet decomposition and sidereal filtering have been employed to denoise the signals and mitigate the negative impact of multipath effects on accurate position tracking. These techniques help to improve the overall performance and reliability of mobile position tracking systems [15, 16].

Broadcom announced the world's first mass-market, dual-frequency GNSS receiver device, the BCM47755, on September 21, 2017. Following this, in May 2018, the Xiaomi Mi8 smartphone became the first to employ a dual-frequency GNSS receiver capable of receiving signals on L1/E1 and L5/E5a frequencies. This advancement in dual-frequency capability led to subsequent studies investigating smartphone-based positioning. The introduction of dual-frequency capability in the Xiaomi Mi8 allowed researchers to examine its multipath performance for both E1/L1 and E5a/L5 signals using appropriate linear combinations. The obtained results were promising, but they also indicated that multipath remains a significant challenge in smartphone positioning. This suggests that multipath interference continues to affect the accuracy and reliability of GNSS positioning on smartphones, even with the advancements in dual-frequency technology.

Some of the experiments are done in Nexus 9 to study multi path effects in Android devices [19]. The study focused on assessing precise positioning using GNSS raw measurements (GPS and GLONASS) from a Nexus 9 tablet under different multipath conditions. The research found that the accuracy of calculated positions was highly influenced by multipath, aligning with previous studies. Without multipath mitigation, significant errors of tens of meters were observed in the code measurements. These errors had a substantial impact on calculated positions even after applying smoothing to the measurements, affecting both standalone positioning (SPP) and differential GNSS (DGNSS) methods. Even after removing most of the multipath interference, the remaining code noise still had a significant impact on the estimated positions. The precision of SPP and DGNSS methods showed a negligible difference. Additionally, the study confirmed the presence of relative receiver code biases in DGNSS with multiple GNSS systems. These biases originated from both GLONASS inter-frequency biases (IFBs) and the inter-system bias (ISB) between GPS and GLONASS code observations.

Environment influences the performance of the GNSS measurement. Code noise can be categorized as either uncorrelated or correlated. Uncorrelated code noise, also known as thermal noise code tracking jitter, is modeled as white-like noise without repetitive patterns over time. This noise and the corresponding error in the pseudorange measurement are caused by thermal electronic noise affecting the correlation process. The uncorrelated code noise is dependent on the specific receiver and antenna being used. The receiver's ability to track a signal and the corresponding uncorrelated code noise error depend on the signal's power. A strong signal leads to low uncorrelated code noise error, while a weak signal results in higher error. The received signal power is influenced by the elevation angle, primarily determined by the receiver antenna's gain pattern. With low antenna gain at low elevations, the signal power is reduced, leading to higher uncorrelated code noise. Conversely, at high elevations, where the antenna gain is higher, the uncorrelated code noise is lower due to the increased signal power.

Multipath refers to the reception of reflected or diffracted signals that create replicas of the desired line-of-sight signal. These replicas are then combined with the direct signal through constructive and destructive interference, resulting in a new composite signal. Unlike uncorrelated code noise, multipath is correlated in time and does not exhibit noise-like behaviour. In the case of static multipath, where a reflected signal interacts with the line-of-sight signal, the composite

signal would either exhibit a constant increase or decrease in C/N0 (carrier-to-noise ratio). However, in reality, GNSS satellites are constantly moving, and the environment is time-varying. As a result, the multipath effect causes sinusoidal variations in the power of the composite signal. The extent of these variations depends on factors such as the distance between the antenna and the reflector, the satellite's elevation and azimuth changes, the carrier signal wavelength, and the vectors of the antenna, reflector, and line-of-sight. The reception of multipath signals distorts the correlation function formed in the receiver with the signal replica, introducing an error in the measured pseudorange. The correlation function is used to determine the timing and phase of the received signal, and the presence of multipath disrupts this process, leading to inaccuracies in the pseudorange measurement.

Receiver noise has significant part in smart phone location tracking. Because smart phones don't use commercial GNSS receiver which provide centimetre level accuracy [7]. This worse quality of the measurement causes many carriers phase cycle slips and increased multi path interference. Measurement errors in receiver may arise from receiver noise, radio frequency interference, and multi path interference which is happened when signals arrived by reflected or diffracted from the local objects not by satellite.

Precise location tracking depends on the elevation and arrangements of the satellites. Fig.1 explain it in below picture [6].

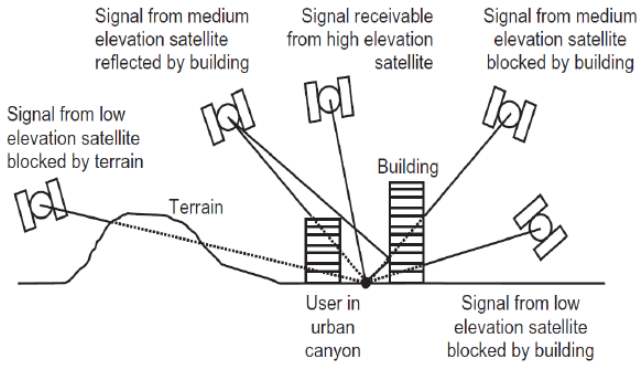

Fig 1: Effect of satellite elevation and arrangement

The key to providing high-accuracy positioning to a wider user base lies in mass-market GNSS receivers that are small and low-cost, integrated into everyday devices such as smartphones, clothes, watches, and cars. Efforts have been made to develop consumer-grade GNSS receivers capable of techniques like lane-level positioning, road user charging, pay-as-you-drive insurance, drone navigation, location-based services, and personal navigation.

Emerging services and applications, such as virtual and augmented reality, safety navigation for visually impaired individuals, and autonomous driving, require centimetre-precision positioning accuracy on affordable mobile platforms. Therefore, the natural progression of this trend involves implementing Real-Time Kinematic (RTK) and/or Precise Point Positioning (PPP) techniques on consumer-grade GNSS receivers and smartphones.

In May 2016, Android developers got access to GNSS raw measurements. This new feature opened up new research possibilities as stated in the GNSS Raw Measurement Task Force's white paper coordinated by the European GNSS Agency (GSA). The availability of GNSS raw measurements in Android enables various research directions. These include optimizing multi-GNSS and multi-frequency solutions, selecting satellites based on performance, transferring processing techniques from dedicated GNSS receivers to smartphones, integrating GNSS raw data with other sensor data available on smartphones, and enabling testing and post-processing analysis. However, the use of GNSS raw measurements presented challenges for both GNSS experts and software developers. GNSS standard formats like RINEX or NMEA are not readily available on the Android platform, requiring conversion or adaptation. Additionally, mobile app developers may not possess familiarity with the complex algorithms and libraries typically used in GNSS positioning [18].

Technically GNSS measurements can be gotten in Android devices through the Android operating system's API. Starting from API level 24, which was introduced in Android 7, users can utilize the GnssMeasurement and GNSSClock classes to access these measurements. The API provides all the necessary components to generate a complete and standardized RINEX (Receiver Independent Exchange) file, which includes code and carrier phase measurements, Doppler information, and the signal-to-noise ratio expressed as C/N0 (dBHz). However, converting the data from the Android format to RINEX is not a straightforward task [17]. One challenge in this conversion process is dealing with the time and distance units provided by Android, which are expressed in nanoseconds. Proper conversion and formatting are required to ensure compatibility with the RINEX format.

In the smart phones, battery life is a one of the import factors. Continuously using GNSS receiver drains the battery. To address this, GNSS chip manufacturers employ a technique called duty-cycling, where the power to the receiver is cycled on and off. This allows the receiver to track GNSS data continuously only for a fixed period known as the burst period, after which the main routines inside the chipset are shut down to conserve power. For reliable testing with GNSS carrier-phase measurements obtained from an Android device, it is necessary to verify if the device has duty-cycle deactivated. Deactivating the duty-cycle enables continuous tracking of the carrier phase without experiencing cycle slips or interruptions in the measurements.

Cycle slip refers to a disruption or error in the measurement of carrier phase in Global Navigation Satellite Systems. In GNSS positioning, carrier phase measurements are used to calculate highly precise position, velocity, and timing information. The carrier phase represents the number of complete wavelengths of the carrier signal between the satellite and the receiver antenna. However, due to various factors such as signal blockage, multipath interference, or receiver noise, the carrier phase measurement can experience sudden discontinuities or shifts. These discontinuities cause a cycle slip, where the receiver loses track of the correct number of cycles of the carrier phase. Cycle slips can significantly affect the accuracy of GNSS positioning solutions. When a cycle slip occurs, the receiver's ability to track the carrier phase accurately is compromised, leading to incorrect positioning results. Therefore, detecting and correcting cycle slips is essential to ensure the reliability and precision of GNSS positioning. Cycle slip detection algorithms analyse the carrier phase measurements to identify the occurrence of cycle slips. Once a cycle slip is detected,

various techniques can be employed to repair or mitigate the impact of the cycle slip. These techniques include using dual-frequency receivers, differencing techniques, or utilizing data from multiple satellites to resolve the cycle slip ambiguity.

GPS signal carrier phase measurements can be used to obtain high-precision positioning and navigation solutions. Measurements of the carrier phase, on the other hand, require the resolution of integer ambiguities. Cycle slips (CSs) can cause errors in carrier phase measurements in Global Navigation Satellite Systems (GNSS), affecting positioning accuracy. Integer ambiguity resolution, which resolves the ambiguity in the number of cycles, can be computationally complex and cause delays. Therefore, detecting and repairing CSs is important. However, CS detection from carrier phase measurements is challenging as it requires additional information like precise positioning or known positions. Various methods combining different instruments have been proposed, but they have limitations in urban environments. Carrier phase measurements offer precise positioning but require a dual-frequency receiver. In some cases, simultaneous cycle slip combinations on different frequencies may not provide information about the phase in which the slip occurred or may be completely missed during detection. Yoon et al proposed a method that utilize a channel-specific technique for the detection of cycle slips in multi-channel systems. The approach involves using ratios to identify cycle slips in each channel individually. By comparing the ratios with the time and range domains, the suggested method enables the detection of small-sized cycle slips simultaneously across multiple channels.

For the single frequency receiver, there are three ways to detect and correct cycle slip. [22] employ the geometry-free approach and apply wavelet transformation for CS detection. [22] use phase-phase combinations, while [23] uses carrier phase measurements alone. For CS correction, [23] and [22] use second-order polynomial fitting. The results of using Sym4 wavelets in [23] show promise, but further extension of the work is not mentioned. The implementations confirm the effectiveness of wavelet usage, but the processing is offline. Additionally, the non-adaptive filter used can treat noisy signals as CS. While the wavelet technique requires multiple data epochs and is unsuitable for real-time applications, it can be useful in post-processed scenarios.

[24] that employ hypothesis testing on the magnitude of least squares (LS) residuals for cycle slip (CS) detection. If the norm of the residual surpasses a threshold, it is considered an outlier and identified as a CS. [24] uses time-differenced (TD) measurements to calculate LS residuals, discarding measurements once a CS is detected. However, CS correction is not performed, and the detection of multiple simultaneous CS (loss of multiple satellite signals) is not explored. In [25], this idea is extended for real-time kinematic (RTK) positioning, incorporating state-parameter predictions of a Kalman Filter (KF) as measurements to enhance observables redundancy. W-test statistics are utilized to detect outlier epochs, representing CS occurrences. The estimated outlier is used for CS repair, although no technique for estimating CS size is provided. The algorithm detects and corrects single-cycle CS, demonstrating successful positioning in kinematic and static experiments with short baselines. However, accuracy declines as baseline length increases, and the algorithm does not address the case of multiple simultaneous CS.

The third method is using Doppler Effect to detect and correct CS. In [26], a CS detection and repair method is proposed for a single-frequency receiver operating in a standalone point positioning (SPP) configuration. The technique combines time-differenced (TD) carrier-phase measurements with Doppler measurements based on a revised oscillator model. The geometric-range variation between GPS satellites and the receiver is determined from Doppler measurements. A TD measurement residual is computed by subtracting the geometric-range variation from the TD measurements, and its root mean square error (RMSE) is used for CS detection. CS are then repaired by rounding. However, as the measurements are not a linear function of Doppler frequency, they are approximated using the trapezoidal integration method, causing the RMSE to increase at lower sampling intervals. The method is tested on both static and kinematic data, but the kinematic data exhibits higher RMSE as the sampling frequency decreases. Moreover, the method only checks for CS within a single cycle and does not discuss the estimation of CS size for slips spanning multiple cycles.

Most of the cycle slip detection and correction methods are focusing on the outdoor positioning environment. However, these existing methods have limitations when it comes to detecting and repairing indoor cycle slips. Some studies have employed Bayesian detection and Doppler integration, but the accuracy is limited at low frequencies. The high-order differences method is simpler but unpredictable at low sampling rates. Polynomial fitting performs well with signal discontinuities but poorly with sampling intervals larger than 1 second. The Melbourne-Wubbena (M-W) linear combination has been widely used, but it is affected by severe multipath effects in ground-based positioning. Code measurement errors can lead to low-accuracy initial cycle slip detection using the M-W combination. A new approach utilizing dual-frequency data from a single GPS receiver is suitable for short sampling periods. Modifications have been proposed, including the use of ionospheric total electron contents rate (TECR) and the time-differenced Hatch-Melbourne-Wübbena (HMW) linear combination. These approaches reduce code measurement noise but may not be applicable to ground-based navigation systems unaffected by the ionosphere.

Zhao et al proposed paper which aims to detect and repair cycle slips in ground-based positioning systems while mitigating the impact of multipath [27]. Unlike many existing methods that use phase/code range combinations, this approach solely relies on phase observations. This enables its suitability for implementation in ground-based systems and offers advantages such as reduced observation noise levels in indoor environments and the ability to accommodate longer sampling intervals. Numerical results demonstrate the effectiveness of the new algorithms in detecting and repairing cycle slips under multipath conditions. The approach incorporates an adaptive weight Particle Swarm Optimization (APSO) algorithm, enabling rapid identification of cycle slip candidates without searching the search space by code range. This capability paves the way for the development of new algorithms specifically designed for repairing cycle slips in indoor navigation scenarios.

Android provide cycle slip flags through their APIs. But the detection mechanism is unknown. Verheyde et al tried to find answer for it. They concluded that the computation processes

used in these mechanisms do not solely rely on naive interpolation of C/N0 (Carrier-to-Noise Density) or satellite elevation parameters [28]. The similarities observed across different smartphone brands suggest that these detection algorithms might be implemented at a low-level Android layer. The paper highlights that the flags indicating multipath tend to be inconsistent, while the cycle slip flags demonstrate more coherence despite their tendency to have a higher false alarm activation frequency. Previous studies conducted in static scenarios have shown that collaborative smartphone positioning is achievable, and GNSS measurements can be effectively modelled. However, the multipath and cycle slip indicators in Android devices may not be suitable as reference parameters for accurately assessing the performance of smartphone positioning.

With the advancements in GNSS systems, the availability of triple-frequency signals has opened up new possibilities for cycle slip detection and repair. Several methods have been proposed to take advantage of these triple-frequency observations. Dai et al. proposed an instantaneous method using two geometry-free phase combinations and the LAMBDA algorithm for cycle slip detection, but it may miss certain undetectable cycle slips. Huang et al developed real-time methods based on triple-frequency observations, assuming smooth ionospheric delay variations, which may be less effective in high ionospheric activity conditions [29]. Zhao et al introduced ionospheric prediction to compensate for ionospheric bias, but these methods require multiple epochs of continuous phase data without cycle slips [30]. Huang et al. utilized geometry-free and ionosphere-free combinations to mitigate ionospheric delay impact, but the success rate of cycle slip detection decreases in the presence of significant pseudorange noise. Zhang extended the geometry-based approach by integrating time-differenced pseudorange and carrier phase observations for estimating the integer number of triple-frequency cycle slips. These methods collectively explore different techniques to detect and repair cycle slips using triple-frequency observations.

Liu et al proposed a new real-time cycle slip detection and repair method is presented specifically designed for undifferenced GPS/BDS triple-frequency observations collected with a single receiver, particularly under high ionospheric activity conditions [31]. The method utilizes three geometry-free pseudorange minus phase combinations that are linearly independent to effectively detect and accurately repair cycle slips in the original triple-frequency carrier phase observations. Additionally, a second-order time-difference algorithm is employed to mitigate the impact of ionospheric variations between epochs, improving the success rate of rounding the estimated float cycle slips. The approach only requires observations from three consecutive epochs, enabling real-time detection and repair of cycle slips. Static experiments conducted during a magnetic storm and kinematic experiments (car-driven and airborne) verify the performance of the method. The results demonstrate that the proposed method can detect and correctly repair cycle slips as small as 1 cycle in real time under high ionospheric activity. Compared to existing double-frequency methods, the proposed method reduces the impact of pseudorange noise due to the longer wavelength of triple-frequency combinations. Moreover, compared to triple-frequency methods utilizing ionospheric prediction, the proposed method requires fewer consecutive epochs. Furthermore, the proposed method does not rely on external information such as precise orbit and clock corrections, unlike the geometry-based time-differential positioning method.

A. Locate Mobile Position

Following equation shows calculation of code pseudo range.

$$P = (t_r + t_s) * C$$

In the above equation, P, t_r, t_s denotes pseudo range, receiver clock reading at reception and satellite clock reading at transmission respectively. C denotes speed of light.

After considering clock errors

$$t_r = t^r + \tau_r$$
$$t_s = t^s + \tau_s$$

t^r, t^s are true receive and transmit time. τ_r, τ_s are clock errors. After substitute this into pseudo range formulae.

$$P = [(t^r + \tau_r) - (t^s + \tau_s)] * C$$
$$P = \rho(t^r, t^s) + (\tau_r - \tau_s) * C$$

$$\rho(t^r, t^s) = \sqrt{(x^s(t^s) - x^r(t^r))^2 + (y^s(t^s) - y^r(t^r))^2 + (z^r(t^r) - z^r(t^r))^2} + (\tau_r - \tau_s) * C$$

x^s, y^s, z^s denotes position of satellite and x^r, y^r, z^r denotes position of user in Earth-cantered, Earth-fixed(ECEF) coordinate system. By using Non-Linear Least Squares method, this non-linear equation can be solved and get user position [3].

B. Kalman Filter

Kalman filter uses for estimate unknown quantity with known entity measurements. It uses Kalman Gain matrix to give weight to new update. Following formulas explain how Kalman filter is working.

$$\hat{x}_{k|k-1} = F_k \hat{x}_{k-1|k-1} + b_{k-1}$$
$$\hat{P}_{k|k-1} = F_k \hat{P}_{k-1|k-1} F_k^T + Q_k$$

State and covariance update

$$z_k = H\hat{x}_{k|k-1} + v_{k-1}$$
$$K_k = \hat{P}_{k-1|k-1} H_k^T (H_k \hat{P}_{k-1|k-1} H_k^T)^{-1}$$
$$\hat{x}_{k|k} = \hat{x}_{k|k-1} + K(z_k - Hx_{k|k-1})$$
$$\hat{P}_{k|k} = (I - K_k H_k) + \hat{P}_{k|k-1}$$

Where:

$\hat{x}$ = State estimate
$\hat{P}$ = Estimate covariance
F = State-transition model
b = State offsets
Q = Covariance of the process noise
H = Observation model
K = Kalman gain
z = Actual measurement
v = Observation noise
I = Identity matrix

User's position and velocity can be estimated using Kalman filter. Contribution of this research is to optimize the parameter for Kalman filter to reach better and accurate position of the user. Rest of the paper explains the methodology and result of this model.

The positioning function in the Internet of Vehicles relies on the use of Global Navigation Satellite Systems (GNSS), Inertial Systems, and cameras. GNSS provides high-precision positioning that is available in all weather conditions, but it is susceptible to signal blockage and interference. On the other hand, the Inertial Navigation System (INS) enables autonomous navigation without external information, offering high short-term accuracy and reliability. However, it suffers from error accumulation over time. To address these limitations, multi-sensor information fusion technology is rapidly advancing. In practical applications, vehicle positioning often employs integrated INS/GNSS navigation and information fusion through a Kalman filter (KF). This approach combines the strengths of GNSS and INS, allowing for improved navigation accuracy and enhanced overall system reliability. The Kalman filter helps in integrating and fusing the information from multiple sensors, compensating for errors and achieving optimal estimation of the vehicle's position. By utilizing the complementary advantages of INS and GNSS and leveraging the Kalman filter, the integrated system can overcome individual limitations and deliver robust and accurate positioning for Internet of Vehicles applications.

Sun et al proposed an improved innovation adaptive Kalman filter (IAKF) is proposed [32]. The algorithm utilizes the innovation to construct a chi-squared test, enabling the identification of abnormal measurement noise. Based on this, the update method for the measurement noise variance matrix is enhanced. When abnormal measurement data is detected, the measurement noise variance matrix is adaptively updated by considering the difference between the current innovation and the mean value of the innovation. This update reflects the impact of the abnormal measurement data, effectively suppressing filtering divergence and enhancing positioning accuracy. Experimental results demonstrate that the proposed algorithm successfully mitigates filtering divergence in the presence of disturbed measurement data. The algorithm exhibits improved adaptiveness and stability, making it a valuable contribution to the development of intelligent traffic positioning systems. Overall, the IAKF approach provides a novel solution by effectively managing abnormal measurement noise and enhancing the performance of integrated navigation systems in challenging urban environments.

INS measurement fusion is one of the methods to improve accuracy of mobile phone position tracking. There are several methods proposed but still there are unsolved problems exist. Because the composition of GPS noise is complex, encompassing not only white noise but also random environmental noise caused by factors such as nearby buildings and electromagnetic interference. Additionally, uncertainties in the INS model and noise further complicate the process of fusing information for estimation. Unfortunately, these challenges have not been adequately addressed. The presence of environmental noise significantly impacts the accuracy of estimation in GPS/INS systems. However, a common oversight is treating GPS and INS noises as synonymous with white noise, disregarding the contribution of environmental noise. As a result, the estimation accuracy is significantly compromised. To improve estimation accuracy in GPS/INS systems, it is crucial to consider and address the influence of environmental noise along with GPS and INS noises. By accounting for all sources of noise and properly modelling their effects, more accurate estimations can be achieved. Liu et al proposed the algorithm is called Innovation Adaptive Estimation Adaptive Kalman Filtering (IAE-AKF) based on memory attenuation. This filter aims to prevent filtering divergence and eliminate the influence of environmental noise. Compared to commonly used fusion approaches like Kalman Filtering and Neural network technology, the IAE-AKF method produces superior results. To effectively utilize newly observed information and mitigate the impact of past data on filtering, the algorithm introduces an attenuation memory factor to the observed sequence of innovation. This factor reduces the influence of historical data. Furthermore, to address the issue of GPS output noise, which includes both white noise and the impact of surrounding factors in urban environments, the method increases the weight of the current measurement value. This adjustment serves as an indicator of variance in the output variation. During the filtering process, the method utilizes the continuously modified observed value to correct uncertain parameters and suppress model noise. Overall, the IAE-AKF algorithm offers improved performance by incorporating memory attenuation and effectively handling environmental noise in the estimation process. It provides a promising approach for robust information fusion and filtering in complex environments.

Machine learning algorithms are inevitable in any domains. In that way, Gao et al argued previous studies have acknowledged that the process noise covariance matrix significantly affects the performance of the Kalman filter (KF) in positioning [34]. However, there is a lack of comprehensive estimation methods that can determine the process noise covariance matrix while maintaining accuracy and robustness. They introduced an adaptive Kalman filter navigation algorithm (RL-AKF) that dynamically adjusts the process noise covariance matrix using the deep deterministic policy gradient (DDPG) method. In the RL-AKF algorithm, the integrated navigation system serves as the environment, and the reward is defined as the opposite of the current positioning error. By employing the DDPG method, the algorithm searches for the most optimal estimation of the process noise covariance matrix within the continuous action space. Reinforcement Learning is a machine learning technique used for solving sequential decision-making problems represented as Markov decision processes (MDPs). By leveraging the trial-and-error method with environmental information, RL demonstrates strong automatic exploitation capabilities. In this context, the proposed adaptive Kalman filter navigation algorithm treats the integrated navigation system as the environment and defines the negative positioning error as the reward. The algorithm utilizes deep deterministic policy gradient to obtain the optimal state estimation, specifically the process noise covariance matrix, within a continuous action space. By employing RL, the algorithm adaptively estimates the process noise covariance matrix based on the positioning accuracy, leading to improved navigation performance. The approach leverages RL's ability to learn from environmental interactions, resulting in an optimal state estimation that enhances the

performance of the Kalman filter. Through extensive experiments, the developed method demonstrates its ability to identify the appropriate Q parameters, leading to improved navigation accuracy.

III. METHODOLOGY

A. Data set Information

Google Smartphone Decimetre Challenge data set consists of drive routes which can be classified as highway, street and downtown. Due to the orbital error and measurement noise, some of the observations are not suitable for prediction. Below observations were already filtered by data set vendor [2].

B. Data Pre-processing

Google Smartphone Decimetre Challenge data set consists of drive routes which can be classified as highway, street and downtown. Due to the orbital error and measurement noise, some of the observations are not suitable for prediction. Below observations were already filtered by data set vendor [2].

- CN0 is less than 20 dB-Hz.
- Received satellite time uncertainty in nanoseconds is larger than 500 nanoseconds.
- Status of code was invalid.

Additionally following invalid observations are removed from data set.

- Carrier frequency error greater than 2.0e6 Hz.
- Satellite Elevation Degree less than 15 degree.
- Pseudo range uncertainty greater than 150 meters.
- Multi path indicator greater than 0.
- Carrier phase uncertainty greater than 0.1 meter.

Raw pseudo range data which is given by satellite should be corrected with noise factors.

$$\rho = \rho_{raw} + SVClockBias - SignalRangeBias - IonosphericDelay - TroposphericDelay$$

Where ρ and SVClockBias represent pseudo range and satellite clock bias.

$$PseudorangeRate = RawPseudorangeRate + Thesatelliteclockdrift$$

Pseudo range Rate is another name for Doppler measurement in ms−1. Velocity of the mobile can be estimated using Doppler effect [9]. According to Android GNSS measurement, manual cycle slips are detected and indicated in Table I which is extracted form Android official page [8]. Invalid or unknown state is not considered by model.

Cycle slip flags are mentioned in Accumulated Delta Range Status field in Android GNSS log file. Carrier phase smoothing can be done between cycle slips. Following equation show how carrier smoothing can be made for given satellite and signal type.

Status	Value	Description
ADR STATE CYCLE SLIP	4	A cycle slip has been detected.
ADR STATE RESET	2	A reset has been detected.
ADR STATE VALID	1	The state is valid.
ADR STATE UNKNOWN	0	The state is invalid or unknown.

TABLE 1 Android Cycle Slip Flag

$$SmoothedPsedorange = AccumulatedDeltaRange + Mean(RawPseudorange - AccumulatedDeltaRange)$$

C. Find Estimated Mobile Location from Pseudo Range Using Weighted Least Square Method

$$\rho(t^r, t^s) = \sqrt{(x^s(t^s) - x^r(t^r))^2 + (y^s(t^s) - y^r(t^r))^2 + (y^s(t^s) - z^r(t^r))^2} + (\tau_r - \tau_s) * C$$

In the above equation, the data set already has smoothed pseudo range(ρ), location of satellite($x^s(t^s)$, $y^s(t^s)$, $y^s(t^s)$) and speed of light(C). But mobile location($x^r(t^r)$, $y^r(t^r)$, $y^r(t^r)$) and clock bias ($\tau_r - \tau_s$) are unknown quantity. To solve this equation, we haves 4 unknown entities then we need at least 4 satellite measurement for single position. This nonlinear equation can be solved using Levenberg-Marquardt algorithm that finds local minimum of the cost function.

Objective function, initial guess, Jacobian matrix, weights and loss function are input parameter of least square method. Position and velocity of the mobile can be calculated from Pseudo Range and Pseudo Range Rate measurements.

$$\sum_{n=1}^{4} \left(\frac{\|\vec{x}_i - \vec{y}\| - \rho_i + b}{\delta\rho}\right)^2 \quad (1)$$

$$\sum_{n=1}^{4} \left(\frac{(\vec{v}_{s,i} - \vec{v}) * \vec{r}_i - \vec{v}_{pr,i}}{\delta v_{pr,i}}\right)^2 \quad (2)$$

$$W_x = \frac{1}{\rho_{uncertainty}} \quad (3)$$

$$W_v = \frac{1}{\rho^r_{uncertainty}} \quad (4)$$

Equation 1 and 2 represents residual function for user position and velocity and Matrix 5 represent Jacobian matrix. Best fitted position, velocity and modified Jacobian matrix, which is Gauss-Newton approximation of the Hessian of the cost function, are output of weighted least square method. Fig.2 shows measurement flows in the model.

$$\begin{bmatrix} \frac{(x_{s1}-x_r)}{\rho_{s1}} & \frac{(y_{s1}-y_r)}{\rho_{s1}} & \frac{(z_{s1}-z_r)}{\rho_{s1}} & C \\ \frac{(x_{s2}-x_r)}{\rho_{s2}} & \frac{(y_{s2}-y_r)}{\rho_{s2}} & \frac{(z_{s2}-z_r)}{\rho_{s2}} & C \\ \frac{(x_{s3}-x_r)}{\rho_{s3}} & \frac{(y_{s3}-y_r)}{\rho_{s3}} & \frac{(z_{s3}-z_r)}{\rho_{s3}} & C \\ \frac{(x_{s4}-x_r)}{\rho_{s4}} & \frac{(y_{s2}-y_r)}{\rho_{s4}} & \frac{(z_{s4}-z_r)}{\rho_{s4}} & C \end{bmatrix} \quad (5)$$

Where:

$\vec{x}_i$ = Satellite position
$\vec{y}$ = Position of the user
ρ_i = Pseudo range
b = Clock bias
$\vec{v}_{s,i}$ = Satellite velocity
$\vec{v}$ = Receiver velocity
$\vec{r}_i$ = Pseudo range rate
$\rho_{uncertainty}$ = Raw Pseudo range Uncertainty
$\rho^r_{uncertainty}$ = Pseudo range Rate Uncertainty

The covariance for each result can be achieved using Equation 6 and 7 where J denotes Jacobian matrix. If the residuals are larger in the solution, then covariance is higher for that result.

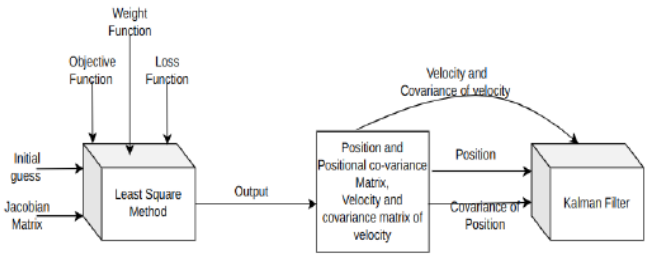

Figure 2 Measurement values for Kalman filter

$$\sigma_x = (J^T \rho_{uncertainty} J)^{-1} \quad (6)$$

$$\sigma_v = (J^T \rho^r_{uncertainty} J)^{-1} \quad (7)$$

D. State Estimation using Kalman Filter

Approximated user position and velocity use as measurement. Following matrices explain the filter procedure. Initial state is set as initial weighted least square approximation value.

$$x = \begin{pmatrix} x_r \\ y_r \\ z_r \end{pmatrix} \quad P = \begin{pmatrix} 25 & 0 & 0 \\ 0 & 25 & 0 \\ 0 & 0 & 25 \end{pmatrix} \quad b = \begin{pmatrix} v_{xr} \\ v_{yr} \\ v_{zr} \end{pmatrix} \quad (8)$$

Rest of the weighted least square approximations use as observation in Kalman filter. σv denotes covariance of velocity and σr denotes covariance of mobile position.

E. Filling Missing Values Using Interpolation

Ground truth of this data set is in Latitude Longitude Height (LLH) coordinates. Then values are transformed from ECEF to LLH coordinate system. For the prediction, we have to fill the missing timelines values using interpolation method.

$$R = \begin{pmatrix} \sigma^v_{xx} & \sigma^v_{xy} & \sigma^v_{xz} \\ \sigma^v_{yx} & \sigma^v_{yy} & \sigma^v_{yz} \\ \sigma^v_{zx} & \sigma^v_{zy} & \sigma^v_{zz} \end{pmatrix} \quad Q = \begin{pmatrix} \sigma^r_{xx} & \sigma^r_{xy} & \sigma^r_{xz} \\ \sigma^r_{yx} & \sigma^r_{yy} & \sigma^r_{yz} \\ \sigma^r_{zx} & \sigma^r_{zy} & \sigma^r_{zz} \end{pmatrix} \quad (9)$$

$$F = \begin{pmatrix} 1 & 0 & 0 \\ 0 & 1 & 0 \\ 0 & 0 & 1 \end{pmatrix} \quad H = \begin{pmatrix} 1 & 0 & 0 \\ 0 & 1 & 0 \\ 0 & 0 & 1 \end{pmatrix} \quad (10)$$

To avoid calculation instabilities, LLH coordinate values are converted in n-vector format. n-vector representation makes calculation simple and non-singular [4].

IV. Result

Estimated data is evaluated based on the Kaggle competition guidelines. Predictions are scored on the mean of the 50th and 95th percentile distance errors. For every phone and once per second, the horizontal distance (in meters) is computed between the predicted latitude/longitude and the ground truth latitude/longitude. These distance errors form a distribution from which the 50th and 95th percentile errors are calculated (i.e. the 95th percentile error is the value, in meters, for which 95% of the distance errors are smaller). The 50th and 95th percentile errors are then averaged for each phone. Lastly, the mean of these averaged values is calculated across all phones in the test set.

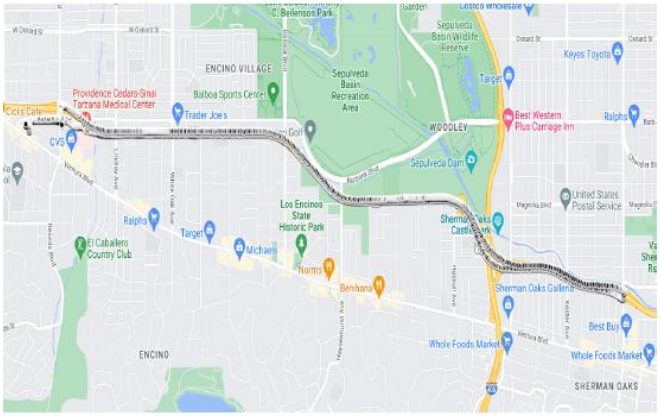

Fig 3: Predicted path for Ventura FWY

Fig.3 shows the ground truth and predicated map for Ventura Free way. Predicted value almost override ground truth. The ground truth data set has speed of the moving mobile phone. The predicted speed can be analysed with Root Mean Square Error (RMSE). Fig.6, the error analysis, shows that there are some sudden spikes in the speed. Ventura FWY is freeway, then this may happen because of high acceleration movement. The model doesn't consider the acceleration entity.

V. Conclusion

Based on the data set vendor's document, user's position is calculated using weighted-Least-Square (WLS) solver and included as ground truth. But proposed model never used the ground truth for any other calculation. Evaluation method performed on the test case and model produced 3.027 meter

positi on accuracy which is more accurate than ground truth.

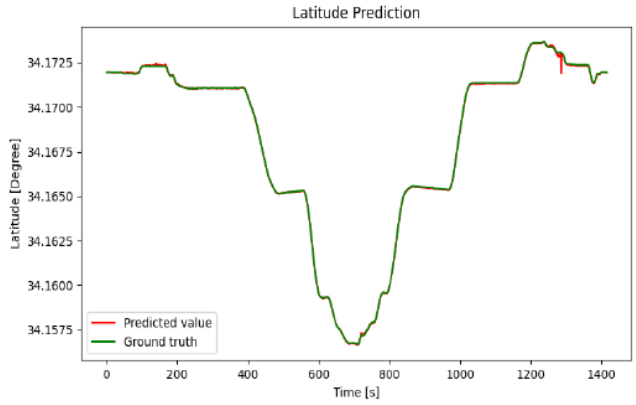

Fig 4: Predicted latitude and ground truth latitude values

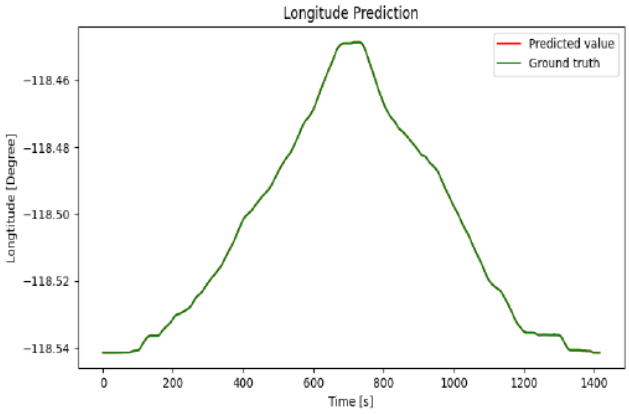

Fig 5: Predicted longitude and ground truth longitude values

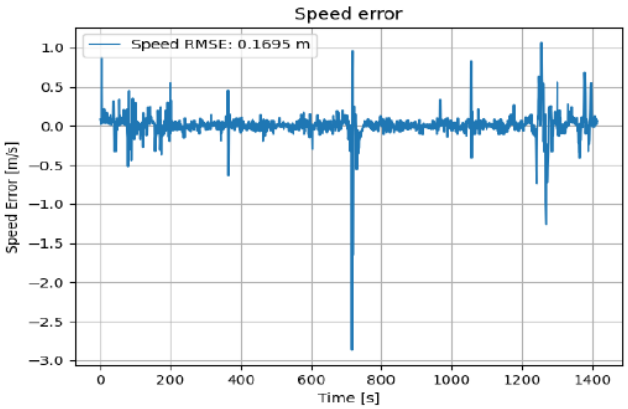

Fig 6: Speed error calculated based on ground truth

Instead of sending raw GNSS measurement data, inserting pre-processed data increase the position accuracy. This position accuracy can be improved by adding additional data such as base station data or Inertial Measurement Unit (IMU) data which adding more entities into the model, such as acceleration, to reach centimetre level accuracy.

REFERENCES

[1] Fu, Guoyu (Michael), Khider, Mohammed, van Diggelen, Frank, Android Raw GNSS Measurement Datasets for Precise Positioning, Proceedings of the 33rd International Technical Meeting of the Satellite Division of The Institute of Navigation (ION GNSS+ 2020), September 2020, pp. 1925-1937.

[2] Fu, Guoyu (Michael), Khider, Mohammed, van Diggelen, Frank, (2022, May), Google Smartphone Decimeter Challenge. Retrieved [Date Retrieved] from https://kaggle.com/competitions/smartphone-decimeter-2022/data.

[3] Kiani Shahvandi, M. and Soja, B., 2022. Inclusion of data uncertainty in machine learning and its application in geodetic data science, with case studies for the prediction of Earth orientation parameters and GNSS station coordinate time series.

[4] Gade, K. (2010). A Non-singular Horizontal Position Representation, The Journal of Navigation, Volume 63, Issue 03, pp 395-417, July 2010.

[5] Error Sources. [online] Available at: ¡https://novatel.com/anintroduction-to-gnss/chapter-4-gnsserror-sources/error-sources¿[Accessed 7 July 2022].s.

[6] Groves, P., 2013. Principles of GNSS, inertial, and multisensor integrated navigation systems. Boston: Artech House.

[7] Everett, T., Taylor, T., Lee, D. and Akos, D., 2022. Optimizing the Use of RTKLIB for Smartphone-Based GNSS Measurements. Sensors, 22(10), p.3825

[8] Android Developers. 2022. Raw GNSS Measurements— Android Developers. [online] Available at:¡https://developer.android.com/guide/topics/sensors/gnss¿ [Accessed7 July 2022]

[9] He, K., n.d. GNSS kinematic position and velocity determination for airborne gravimetry

[10] M. Karaim, M. Elsheikh, and A. Noureldin, ”GNSS Error Sources”, in Multifunctional Operation and Application of GPS. London, United Kingdom: IntechOpen, 2018 [Online]. Available: https://www.intechopen.com/chapters/60049 doi: 10.5772/intechopen.75493

[11] Yang, H., Yang, X., Sun, B. and Su, H., 2016. Global navigation satellite system multipath mitigation using a wave-absorbing shield. Sensors, 16(8), p.1332.

[12] Geng, J. and Bock, Y., 2013. Triple-frequency GPS precise point positioning with rapid ambiguity resolution. Journal of geodesy, 87, pp.449-460.

[13] Wu, X., Zhou, J., Wang, G., Hu, X. and Cao, Y., 2012. Multipath error detection and correction for GEO/IGSO satellites. Science China Physics, Mechanics and Astronomy, 55, pp.1297-1306.

[14] Seepersad, G. and Bisnath, S., 2015. Reduction of PPP convergence period through pseudorange multipath and noise mitigation. GPS Solutions, 19, pp.369-379.

[15] Wang, G., de Jong, K., Zhao, Q., Hu, Z. and Guo, J., 2015. Multipath analysis of code measurements for BeiDou geostationary satellites. GPS solutions, 19, pp.129-139.

[16] Wang, M., Chai, H., Liu, J. and Zeng, A., 2016. BDS relative static positioning over long baseline improved by GEO multipath mitigation. Advances in Space Research, 57(3), pp.782-793.

[17] Pirazzi, G., Mazzoni, A., Biagi, L. and Crespi, M., 2017, September. Preliminary performance analysis with a GPS+ Galileo enabled chipset embedded in a smartphone. In Proceedings of the 30th International technical meeting of the satellite Division of the Institute of Navigation (ION GNSS+ 2017) (pp. 101-115).

[18] Benvenuto, L., Cosso, T. and Delzanno, G., 2022. An Adaptive Algorithm for Multipath Mitigation in GNSS Positioning with Android Smartphones. Sensors, 22(15), p.5790.

[19] Håkansson, M., 2019. Characterization of GNSS observations from a Nexus 9 Android tablet. GPS solutions, 23(1), p.21.

[20] Benvenuto, L., Dabove, P., Ferrando, I. and Sguerso, D., 2021. Preliminary results on tropospheric ZTD estimation by smartphone. Remote Sensing, 13(22), p.4567.

[21] Yoon, Y.M., Lee, B.S. and Heo, M.B., 2022. Multiple Cycle Slip Detection Algorithm for a Single Frequency Receiver. Sensors, 22(7), p.2525.

[22] Wang, B., Chen, D. and Bian, H., 2011, May. Cycle slips detection and repairing to GPS phase observation based on sym4 wavelet. In 2011 International Conference on Multimedia and Signal Processing (Vol. 1, pp. 329-333). IEEE.

[23] Jia, P.Z., 2001. An algorithm for detecting and estimating cycle slips in single-frequency GPS. Chinese Astronomy and Astrophysics, 25(4), pp.515-521.

[24] Kirkko-Jaakkola, M., Traugott, J., Odijk, D., Collin, J., Sachs, G. and Holzapfel, F., 2009, October. A RAIM approach to GNSS outlier and cycle slip detection using L1 carrier phase time-differences. In 2009 IEEE Workshop on Signal Processing Systems (pp. 273-278). IEEE.

[25] Lin, S.G. and Yu, F.C., 2013. Cycle slips detection algorithm for low cost single frequency GPS RTK positioning. Survey Review, 45(330), pp.206-214.

[26] Ren, Z., Li, L., Zhong, J., Zhao, M. and Shen, Y., 2011. A real-time cycle-slip detection and repair method for single frequency GPS receiver. Int. Proc. Comput. Sci. Inf. Technol, 17, pp.224-230.

[27] Zhao, X., Niu, Z., Li, G., Shuai, Q. and Zhu, B., 2020. A new cycle slip detection and repair method using a single receiver's single station B1 and L1 frequencies in ground-based positioning systems. Sensors, 20(2), p.346.

[28] Verheyde, T., Blais, A., Macabiau, C. and Marmet, F.X., 2020, June. Analyzing android gnss raw measurements flags detection mechanisms for collaborative positioning in urban environment. In 2020 International Conference on Localization and GNSS (ICL-GNSS) (pp. 1-6). IEEE.

[29] Huang, L., Lu, Z., Zhai, G., Ouyang, Y., Huang, M., Lu, X., Wu, T. and Li, K., 2016. A new triple-frequency cycle slip detecting algorithm validated with BDS data. GPS solutions, 20(4), pp.761-769.

[30] Yao, Y.F., Gao, J.X., Wang, J., Hu, H. and Li, Z.K., 2016. Real-time cycle-slip detection and repair for BeiDou triple-frequency undifferenced observations. Survey Review, 48(350), pp.367-375.

[31] Liu, W., Jin, X., Wu, M., Hu, J. and Wu, Y., 2018. A new real-time cycle slip detection and repair method under high ionospheric activity for a triple-frequency GPS/BDS receiver. Sensors, 18(2), p.427.

[32] Sun, B., Zhang, Z., Qiao, D., Mu, X. and Hu, X., 2022. An Improved Innovation Adaptive Kalman Filter for Integrated INS/GPS Navigation. Sustainability, 14(18), p.11230.

[33] Liu, Y., Fan, X., Lv, C., Wu, J., Li, L. and Ding, D., 2018. An innovative information fusion method with adaptive Kalman filter for integrated INS/GPS navigation of autonomous vehicles. Mechanical Systems and Signal Processing, 100, pp.605-616.

[34] Gao, X., Luo, H., Ning, B., Zhao, F., Bao, L., Gong, Y., Xiao, Y. and Jiang, J., 2020. RL-AKF: An adaptive kalman filter navigation algorithm based on reinforcement learning for ground vehicles. Remote Sensing, 12(11), p.1704.